Supporting Information

Redox mediated enhancement and quenching of co-reactant electrochemiluminescence by iridium(III) complexes

Steven J. Blom,[a,†] Natasha S. Adamson,[a,†] Emily Kerr,[b] Egan H. Doeven,[a] Oliver S. Wenger,[c] Raoul S. Schaer,[c] David J. Hayne,[b] Francesco Paolucci,[d] Neso Sojic,[e] Giovanni Valenti,[d] Paul S. Francis[a,*]

[a]Deakin University, Centre for Sustainable Bioproducts, Faculty of Science, Engineering and Built Environment, Geelong, Victoria 3220, Australia.

[b]Institute for Frontier Materials, Deakin University, Geelong, Victoria 3220, Australia.

[c]Department of Chemistry, University of Basel, St. Johanns-Ring 19, 4056 Basel, Switzerland.

[d]Department of Chemistry Giacomo Ciamician, University of Bologna, via Selmi 2, Bologna 40126, Italy.

[e]Univ. Bordeaux, CNRS, Bordeaux INP, Institut des Sciences Moléculaires, UMR 5255, 33607 Pessac, France.

†These authors contributed equally.

Figure S1. (a) Electrochemical potential and ECL measurement sequence used to obtain co-reactant ECL spectra between 0.7 V and 1.6 V vs Ag/AgCl. (b) 'Spooling ECL' plot of the spectra collected for a solution of 1 μM $[Ru(bpy)_3]^{2+}$ and 100 μM $[Ir(sppy)_3]^{3-}$ in ProCell as an example. (c) Contour plot using the same data.

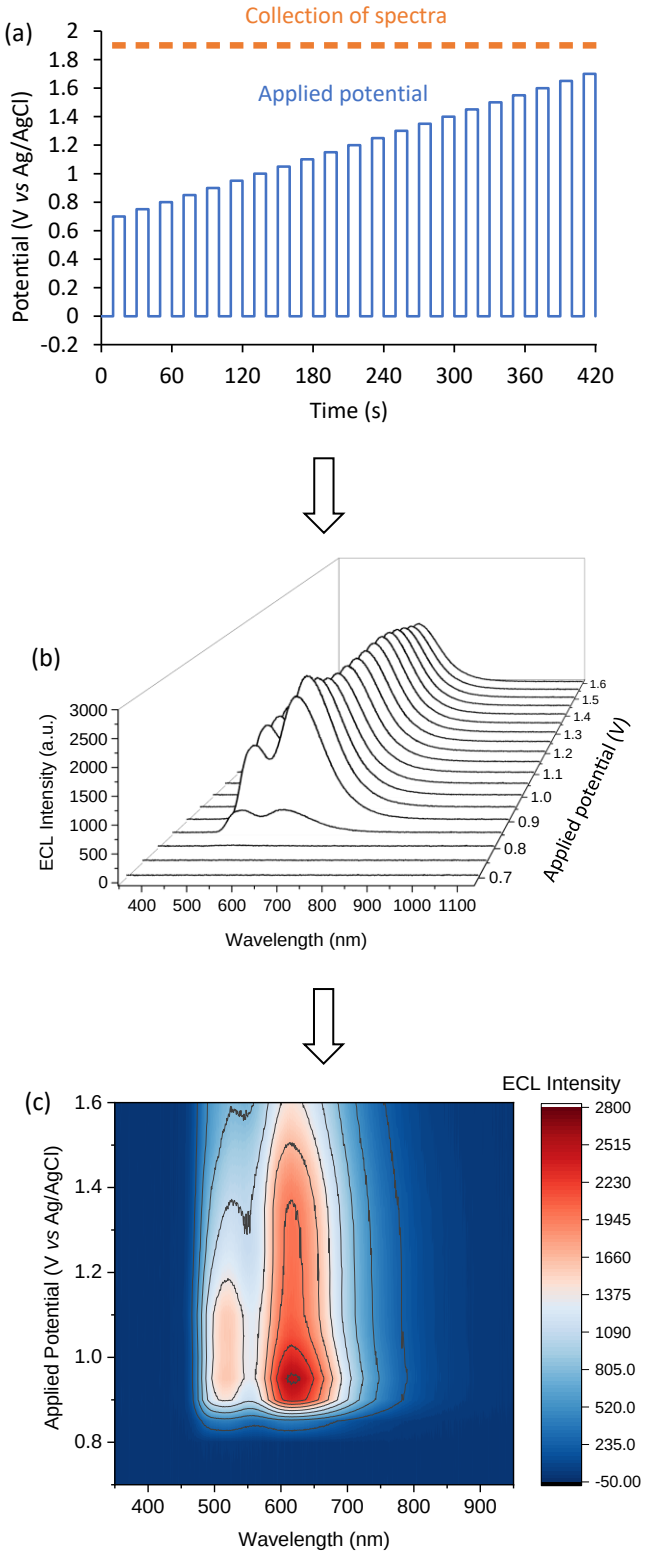

Figure S2. Procedure to create ECL intensity *versus* applied potential plots for each luminophore of a mixture, using the spectra collected for a solution of 1 μM $[Ru(bpy)_3]^{2+}$ and 100 μM $[Ir(sppy)_3]^{3-}$ in ProCell as an example. (a) Spectra generated using the applied potential and ECL measurement sequence shown in Figure S1. (b) Deconvolution of the spectra into the characteristic emission bands of the two metal complexes, using the Solver function of Excel. (c) Each spectrum is then integrated to give the total ECL intensity, which is plotted against the applied potential. The red plot in this case is the 'enhanced' emission of the $[Ru(bpy)_3]^{2+}$. In the main text this is generally compared to the $[Ru(bpy)_3]^{2+}$ ECL intensity without any enhancer, which is obtained through the same process (Figures S1 and S2), except that the deconvolution step is not required.

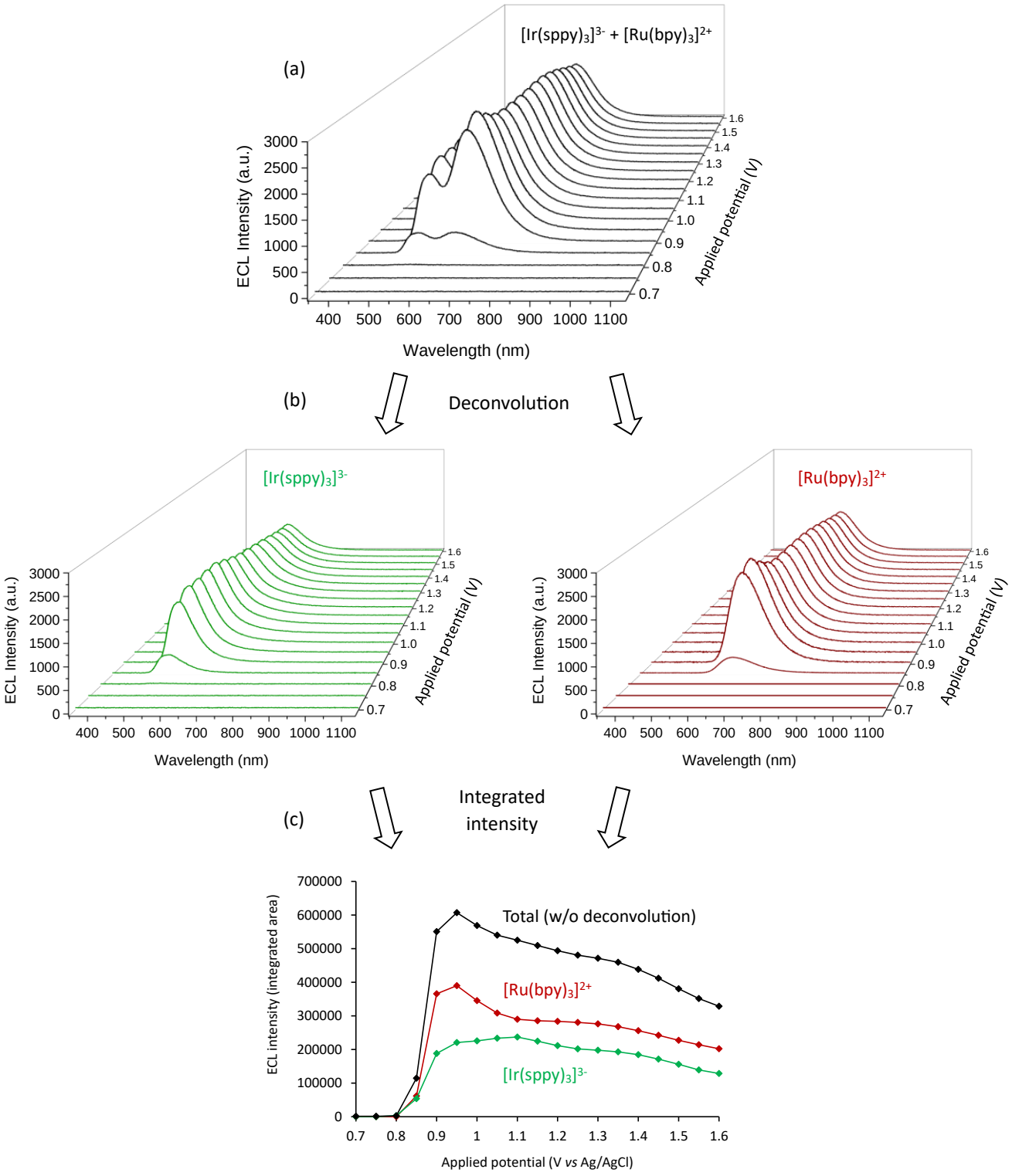

Figure S3. Absorption spectra of (a) $[Ru(bpy)_3]^{2+}$, (b) $[Ir(df\text{-}ppy)_2(pt\text{-}TEG)]^{+}$ (dark blue plot), $[Ir(ppy)_2(pt\text{-}TEG)]^{+}$ (green plot), $[Ir(bt)_2(pt\text{-}TEG)]^{+}$ (orange plot), (c) $[Ir(df\text{-}sppy)_3]^{3-}$ (dark blue plot), $[Ir(f\text{-}sppy)_3]^{3-}$ (light blue plot), and $[Ir(sppy)_3]^{3-}$ (green plot), at 10 μM in water.

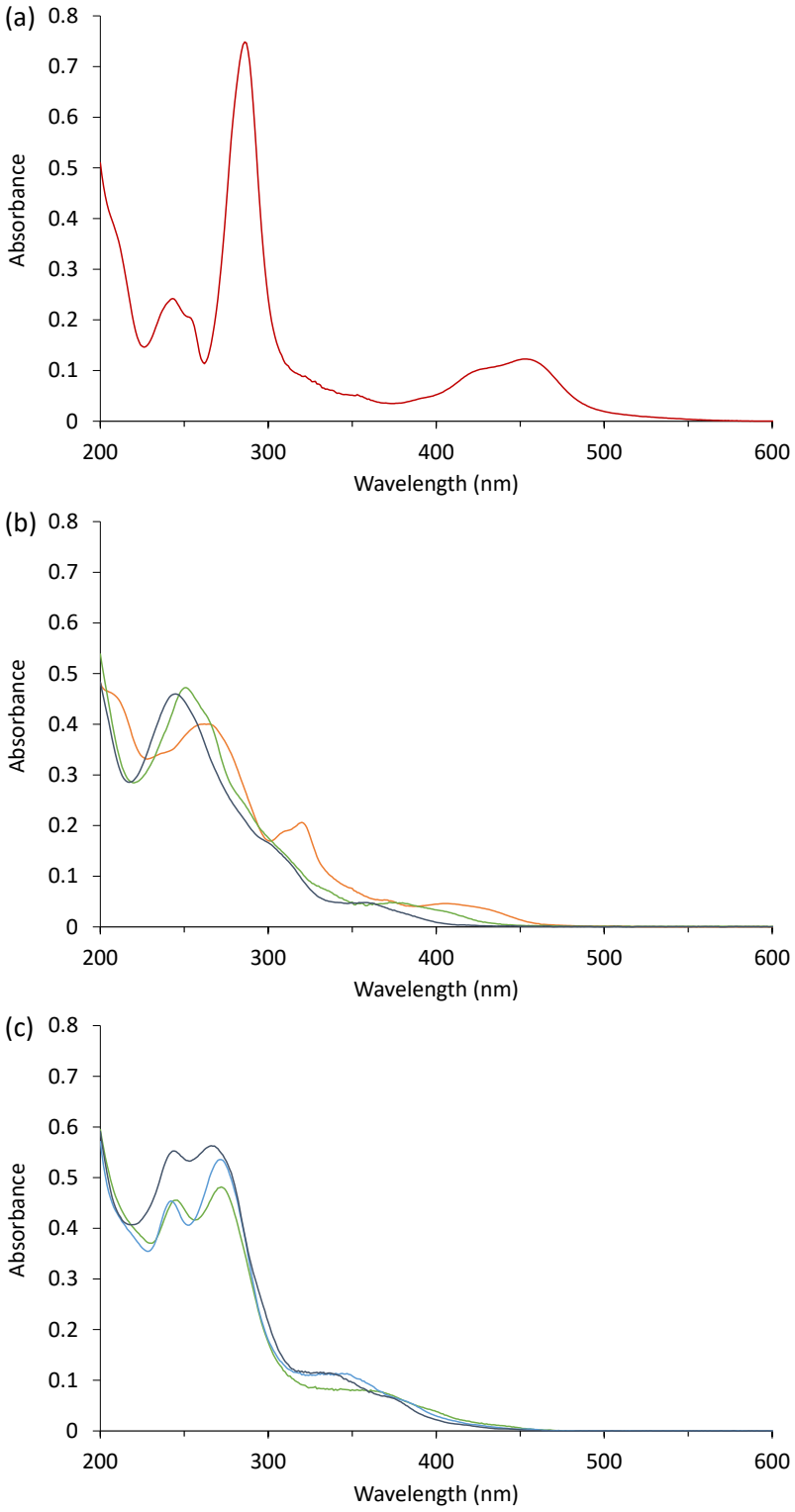

Figure S4. Photoluminescence emission spectra of (a) $[Ru(bpy)_3]^{2+}$, (b) $[Ir(df\text{-}ppy)_2(pt\text{-}TEG)]^{+}$ (dark blue plot), $[Ir(ppy)_2(pt\text{-}TEG)]^{+}$ (green plot), $[Ir(bt)_2(pt\text{-}TEG)]^{+}$ (orange plot), (c) $[Ir(df\text{-}sppy)_3]^{3-}$ (dark blue plot), $[Ir(f\text{-}sppy)_3]^{3-}$ (light blue plot), and $[Ir(sppy)_3]^{3-}$ (green plot), at 10 μM in water. Spectra were corrected for the variation in instrumental sensitivity over the wavelength range.

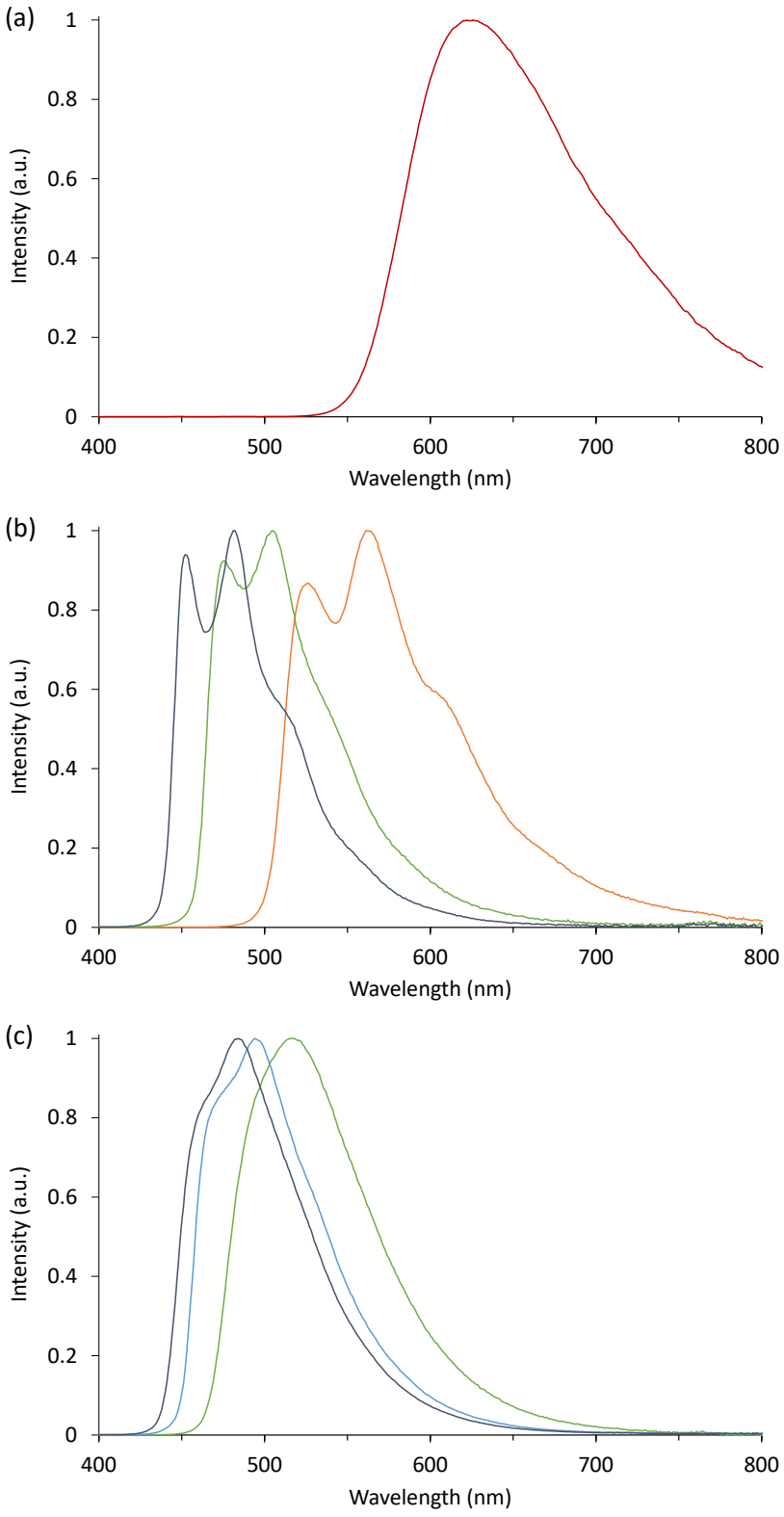

Figure S5. Low temperature (85 K) photoluminescence emission spectra of (a) $[Ru(bpy)_3]^{2+}$, (b) $[Ir(df\text{-}ppy)_2(pt\text{-}TEG)]^+$ (dark blue plot), $[Ir(ppy)_2(pt\text{-}TEG)]^+$ (green plot), $[Ir(bt)_2(pt\text{-}TEG)]^+$ (orange plot), (c) $[Ir(df\text{-}sppy)_3]^{3-}$ (dark blue plot), $[Ir(f\text{-}sppy)_3]^{3-}$ (light blue plot), and $[Ir(sppy)_3]^{3-}$ (green plot), at 10 μM in 4:1 ethanol:methanol. Spectra were corrected for the variation in instrumental sensitivity over the wavelength range.

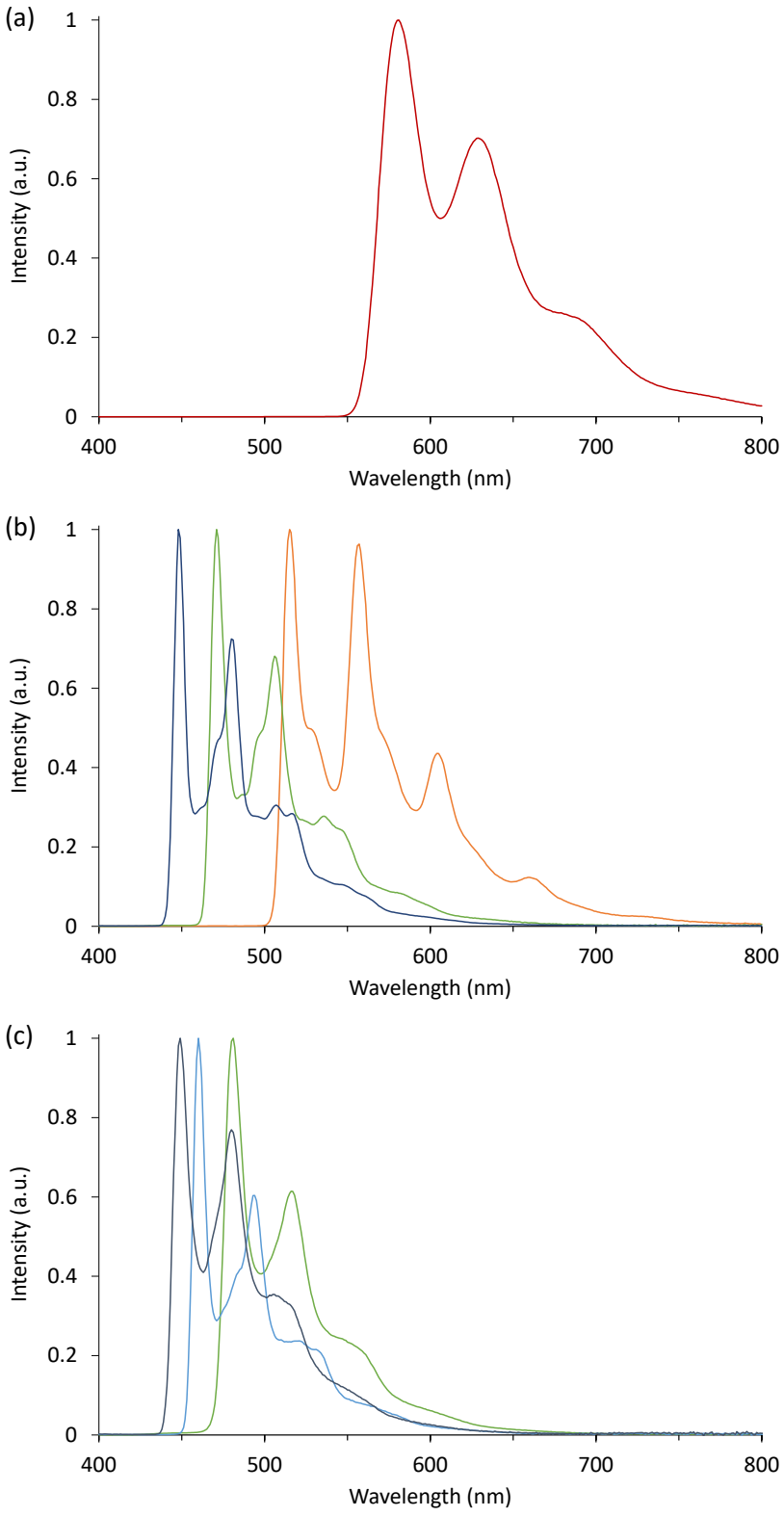

Table S1. Excited state reduction potentials estimated from the ground state potentials and the $E_{0\text{-}0}$ obtained from low temperature emission spectra.[a]

	$E(M^{0*/-})$ / V (vs Ag/AgCl)[b]	$E(M^{+/0*})$ / V (vs Ag/AgCl)[c]
$[Ru(bpy)_3]^{2+}$	0.78	-1.05
$[Ir(bt)_2(pt\text{-}TEG)]^{+}$	0.74	-1.13
$[Ir(df\text{-}ppy)_2(pt\text{-}TEG)]^{+}$	1.02	-1.33
$[Ir(ppy)_2(pt\text{-}TEG)]^{+}$	0.81	-1.55
$[Ir(sppy)_3]^{3-}$	0.53	-1.79
$[Ir(f\text{-}sppy)_3]^{3-}$	0.53	-1.77
$[Ir(df\text{-}sppy)_3]^{3-}$	0.68	-1.68

[a]It should be noted that many of the ground state potentials used to derive these values were estimated from voltammograms of irreversible electron transfers and/or non-aqueous solvents (see Table 1), which increases their margin of error. Even without these considerations, uncertainty in these calculations of 100 mV or more has been reported [1]. [b]Estimated using $E(M^{0*/-}) = E(M^{0/-}) + E_{0\text{-}0}$. [c]Estimated using $E(M^{+/0*}) = E(M^{+/0}) + E_{0\text{-}0}$. As a first approximation, we have omitted the electrostatic work term describing charge generation and separation within the electron-transfer complex.

Figure S6. Cyclic voltammetry (red plots) and squarewave voltammetry (blue plots) for the oxidation of (a) $[Ru(bpy)_3]^{2+}$, (b) $[Ir(bt)_2(pt\text{-}TEG)]^+$, (c) $[Ir(ppy)_2(pt\text{-}TEG)]^+$, and (d) $[Ir(df\text{-}ppy)_2(pt\text{-}TEG)]^+$, in aqueous phosphate buffer (0.1 M, pH 7.5) [2].

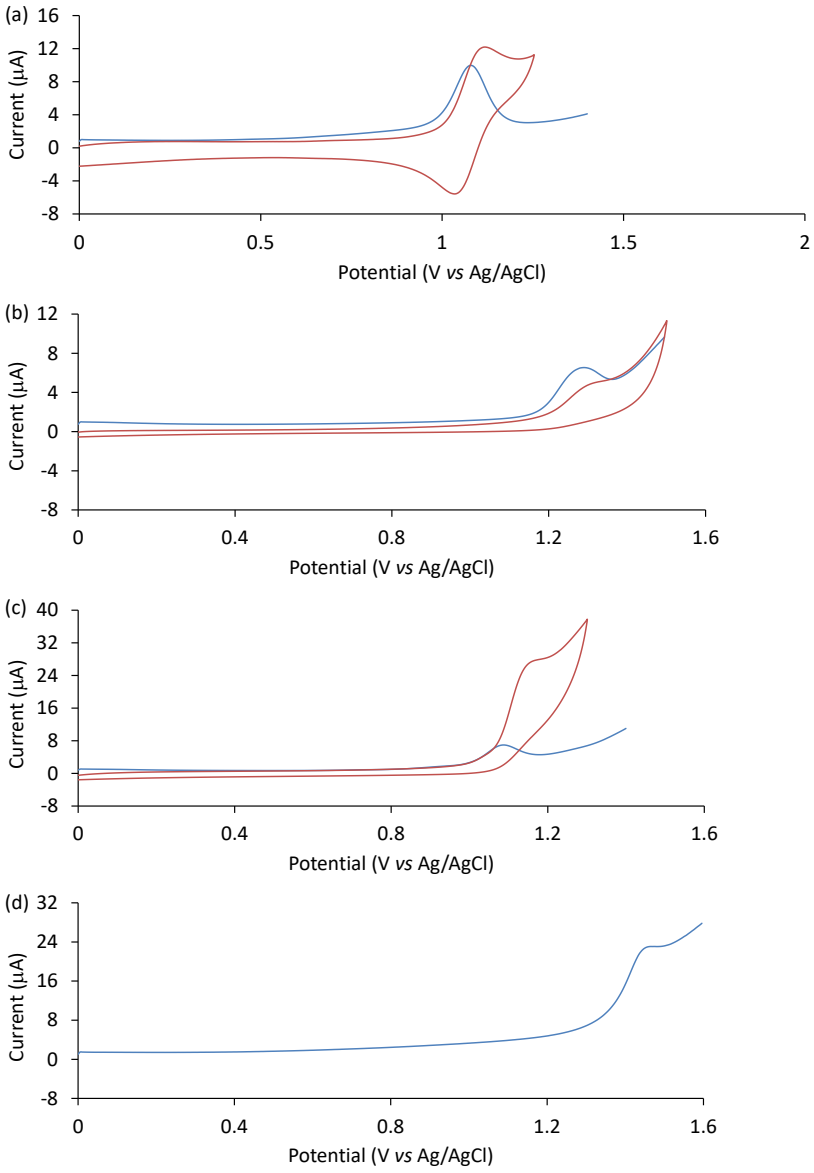

Figure S7. Cyclic voltammetry for the reduction of (a) $[Ru(bpy)_3]^{2+}$, (b) $[Ir(bt)_2(pt\text{-}TEG)]^+$, (c) $[Ir(ppy)_2(pt\text{-}TEG)]^+$, and (d) $[Ir(df\text{-}ppy)_2(pt\text{-}TEG)]^+$ in acetonitrile with 0.1 M $TBAPF_6$ [2].

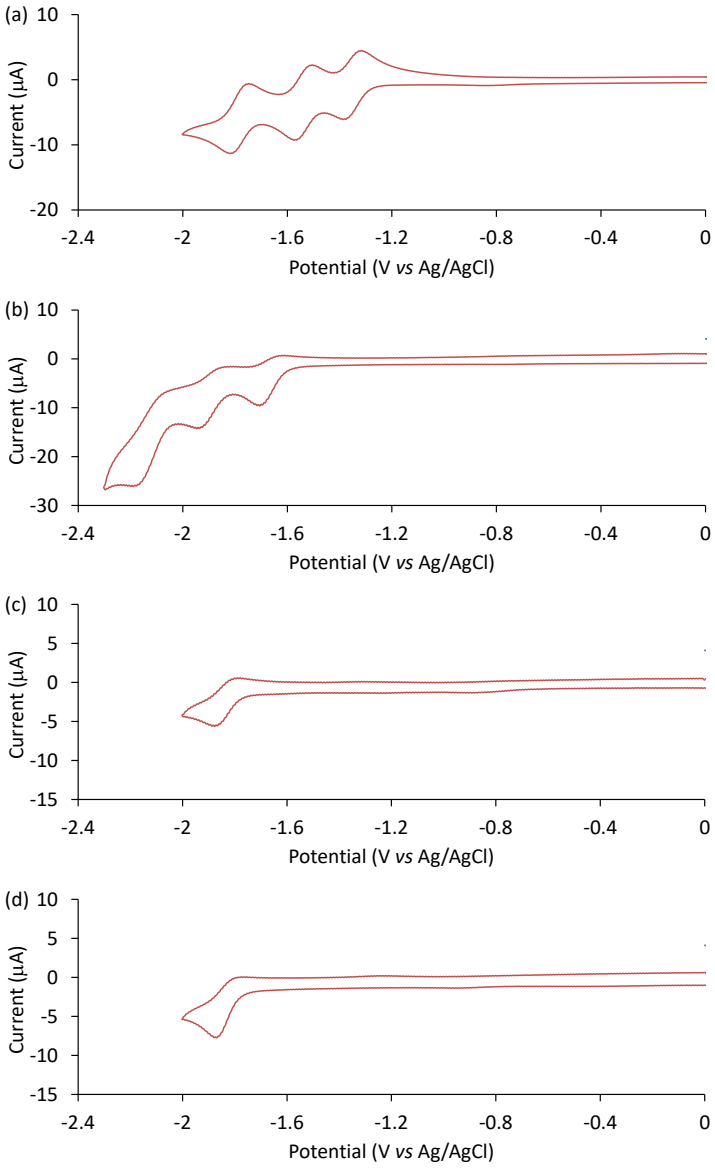

Figure S8. Cyclic voltammetry for the oxidation of (a) $[Ir(sppy)_3]^{3-}$ (b) $[Ir(f\text{-}sppy)_3]^{3-}$, and (c) $[Ir(df\text{-}sppy)_3]^{3-}$, in aqueous phosphate buffer (0.1 M, pH 7.5).

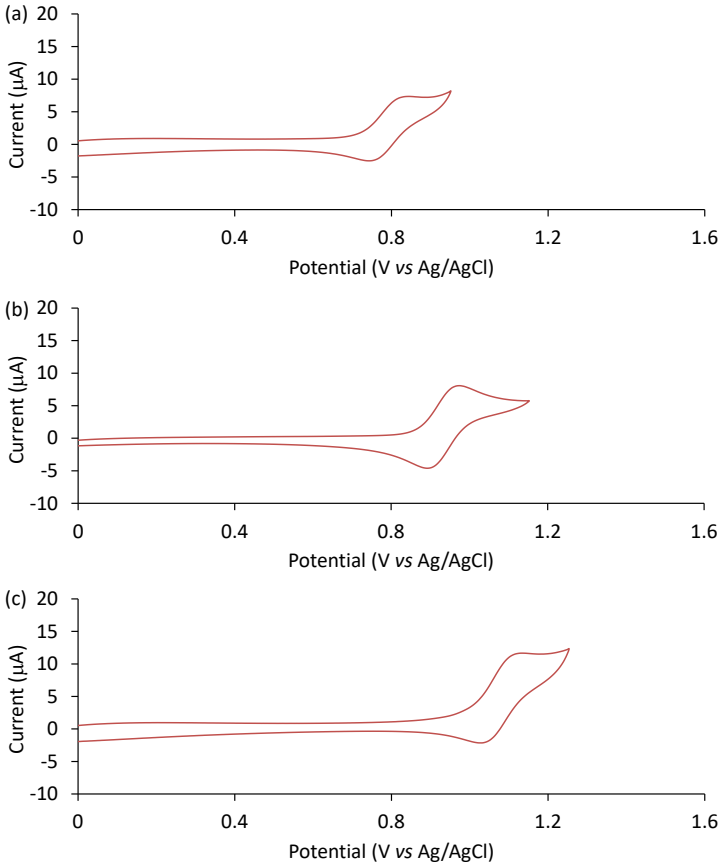

Figure S9. Cyclic voltammetry (red plots) and squarewave voltammetry (blue plots) for the reduction of (a) $[Ir(sppy)_3]^{3-}$ (b) $[Ir(f\text{-}sppy)_3]^{3-}$, and (c) $[Ir(df\text{-}sppy)_3]^{3-}$, in dimethylformamide with 0.1 M $TBAPF_6$.

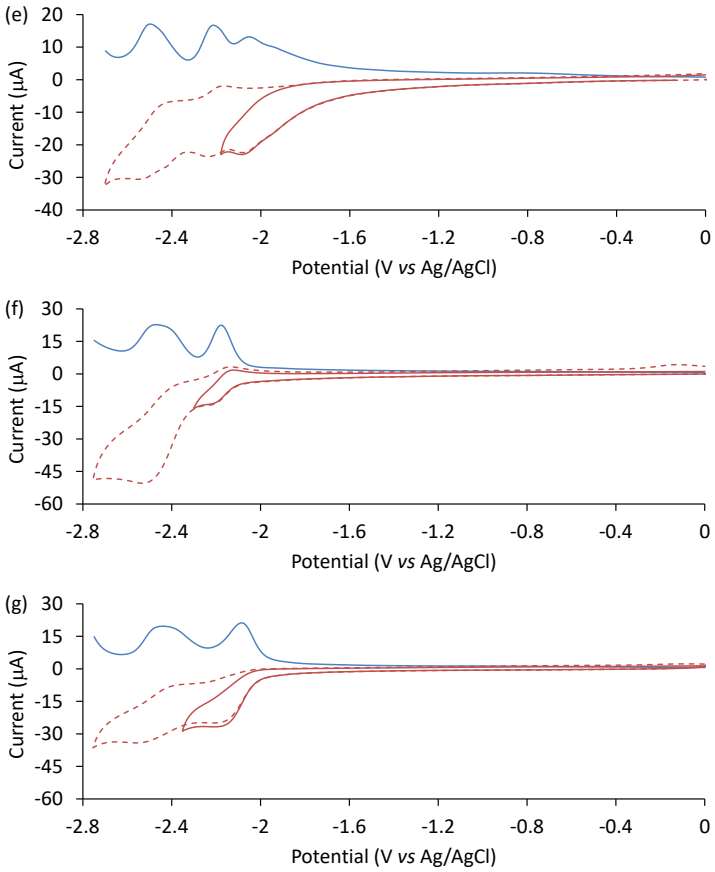

Figure S10. Electrochemiluminescence intensity of (a) $[Ru(bpy)_3]^{2+}$ (red plot), $[Ir(df\text{-}sppy)_3]^{3-}$ (dark blue plot), $[Ir(f\text{-}sppy)_3]^{3-}$ (light blue plot), and $[Ir(sppy)_3]^{3-}$ (green plot), at 2.5 μM in ProCell (180 mM TPrA, pH 6.8). Pulse sequence: 0.9 s at 1.2 V vs Ag/AgCl, then 0.1 s at 0 V vs Ag/AgCl, repeated 9 times. Points represent integrated ECL intensity acquired using an extended range PMT over each 0.9 s pulse time. All RSD ≤ 7% (n = 3). (b) The low intensity portion of the same data. Relative intensities (sum of 9 peaks) are shown in Table S1.

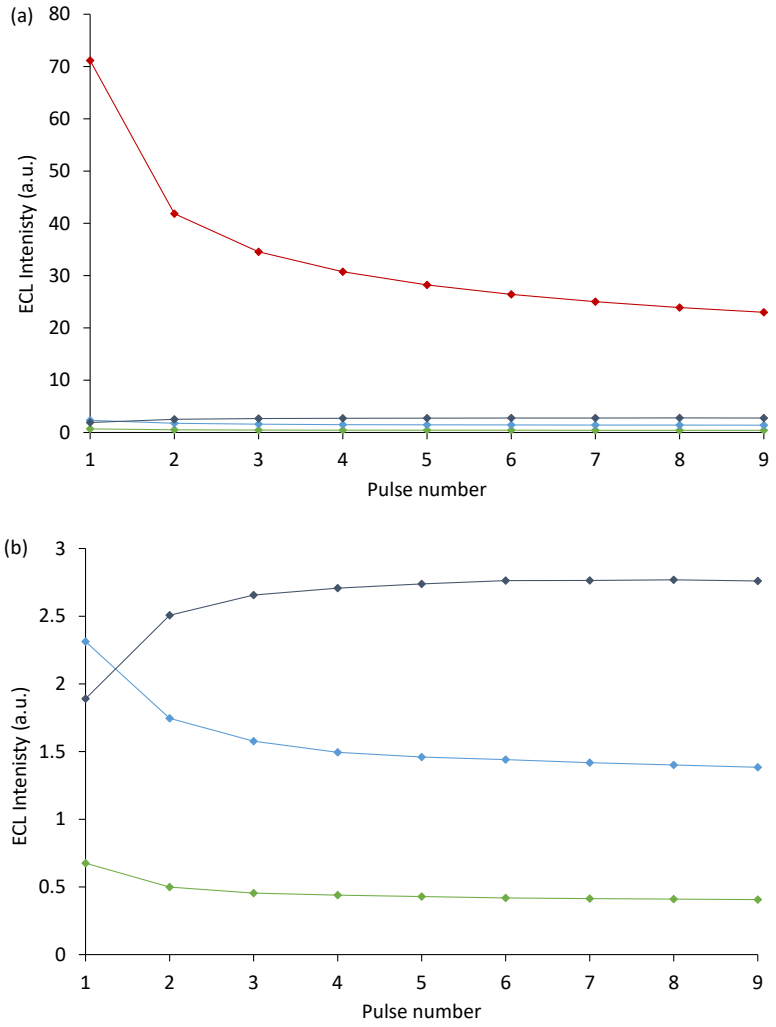

Figure S11. Electrochemiluminescence spectra of (a) $[Ru(bpy)_3]^{2+}$ (red plot), $[Ir(df\text{-}sppy)_3]^{3-}$ (dark blue plot), $[Ir(f\text{-}sppy)_3]^{3-}$ (light blue plot), and $[Ir(sppy)_3]^{3-}$ (green plot), at 10 μM in ProCell (180 mM TPrA, pH 6.8). Applied potential: 1.2 V vs Ag/AgCl for 10 s. Spectra were acquired a CCD spectrometer. (b) The low intensity portion of the same data. Relative intensities (integrated spectra) are shown in Table S1. All RSD ≤ 5% (n = 3).

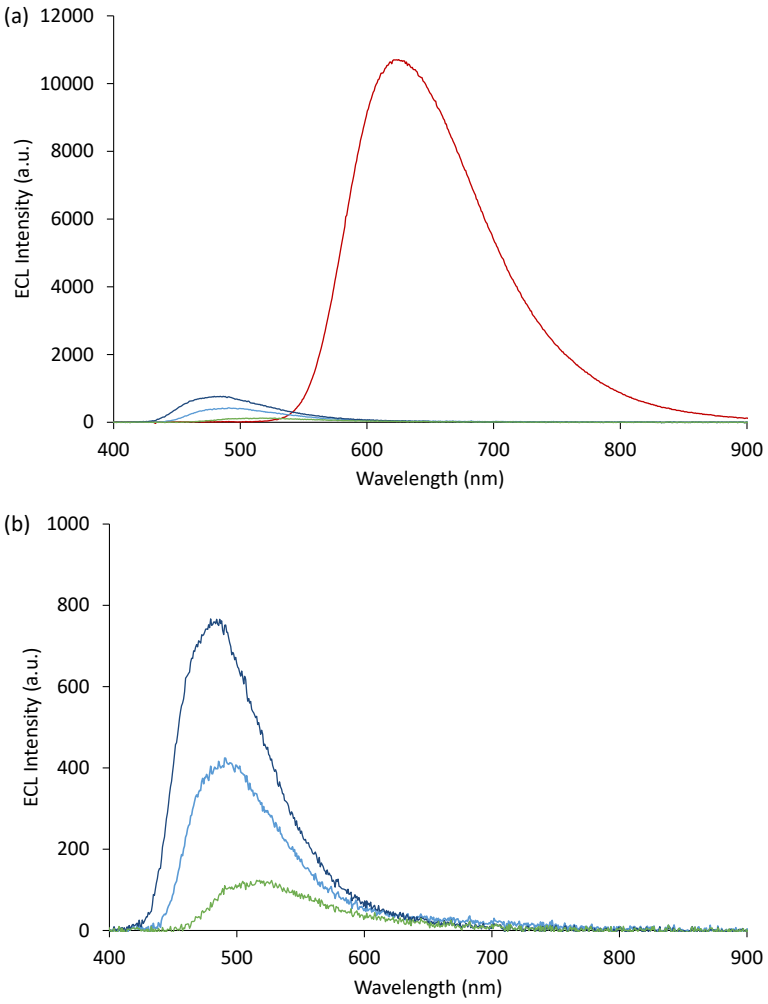

Table S2. Relative intensities of $[Ir(sppy)_3]^{3-}$ and its derivatives with TPrA as co-reactant.

	Relative ECL Intensity vs $[Ru(bpy)_3]^{2+}$		Photo of ECL at working electrode surface
	PMT detector[a]	CCD spectrometer[b]	
$[Ir(sppy)_3]^{3-}$	1.4%	0.9%	
$[Ir(f\text{-}sppy)_3]^{3-}$	4.7%	2.8%	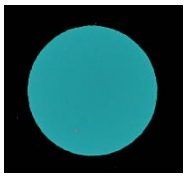
$[Ir(df\text{-}sppy)_3]^{3-}$	7.7%	4.8%	

[a]2.5 μM metal complex in ProCell (180 mM TPrA, 0.3 M phosphate buffer, pH 6.8). Integrated ECL intensity (RSD ≤ 7%; n = 3) over time (pulse sequence: 0.9 s at 1.2 V vs Ag/AgCl, then 0.1 s at 0 V vs Ag/AgCl, repeated 9 times). [b]10 μM metal complex in ProCell. Integrated ECL spectra (RSD ≤ 5%; n = 3) acquired over 10 s at an applied potential of 1.2 V vs Ag/AgCl.

Figure S12. ECL contour plots of (i) 1 μM $[Ru(bpy)_3]^{2+}$, (ii) 1 μM $[Ru(bpy)_3]^{2+}$ and 100 μM Ir(III) complex, and (iii) 100 μM Ir(III) complex, in ProCell solution, where the Ir(III) complex is (a) $[Ir(sppy)_3]^{3-}$, (b) $[Ir(f\text{-}sppy)_3]^{3-}$, or (c) $[Ir(df\text{-}sppy)_3]^{3-}$.

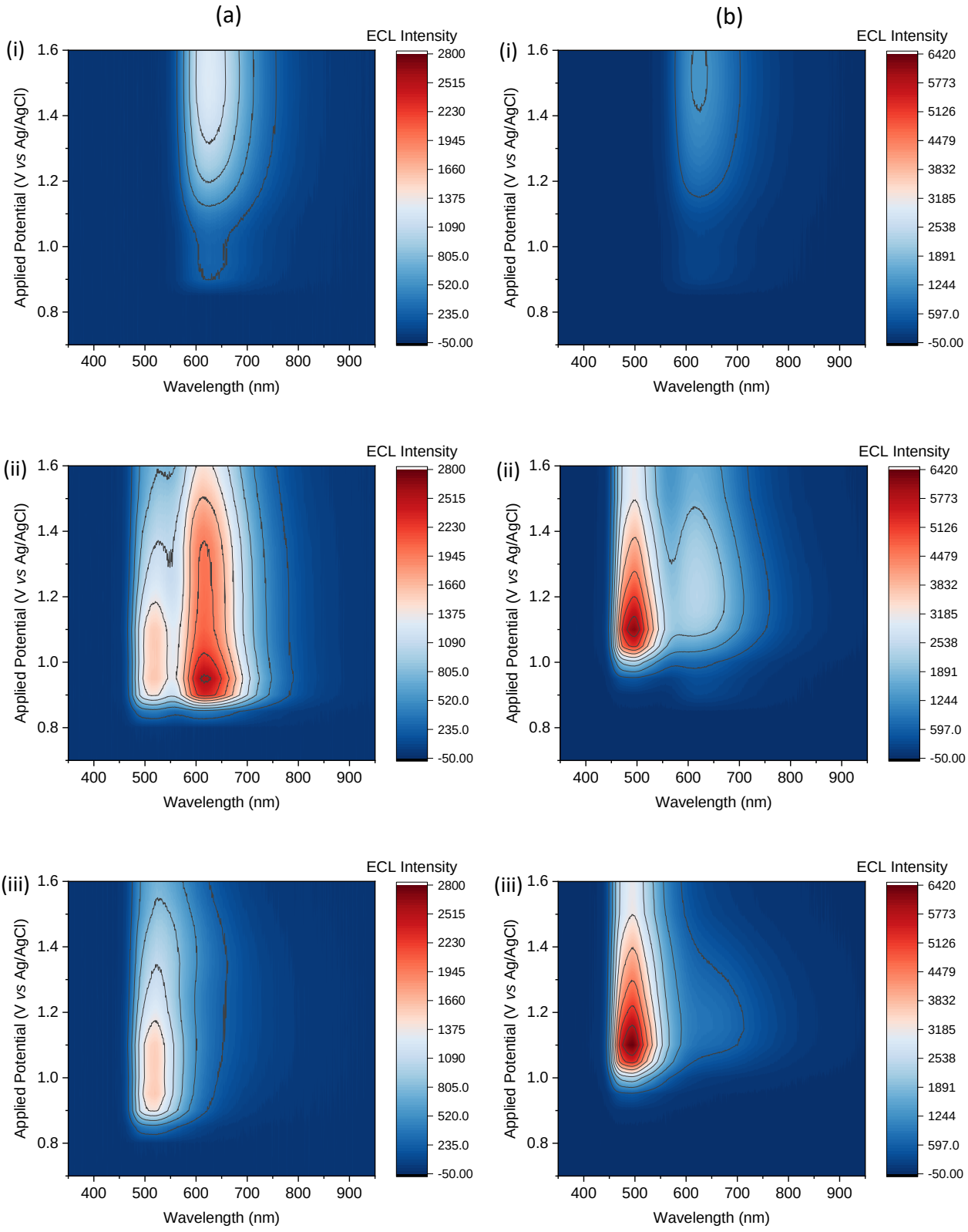

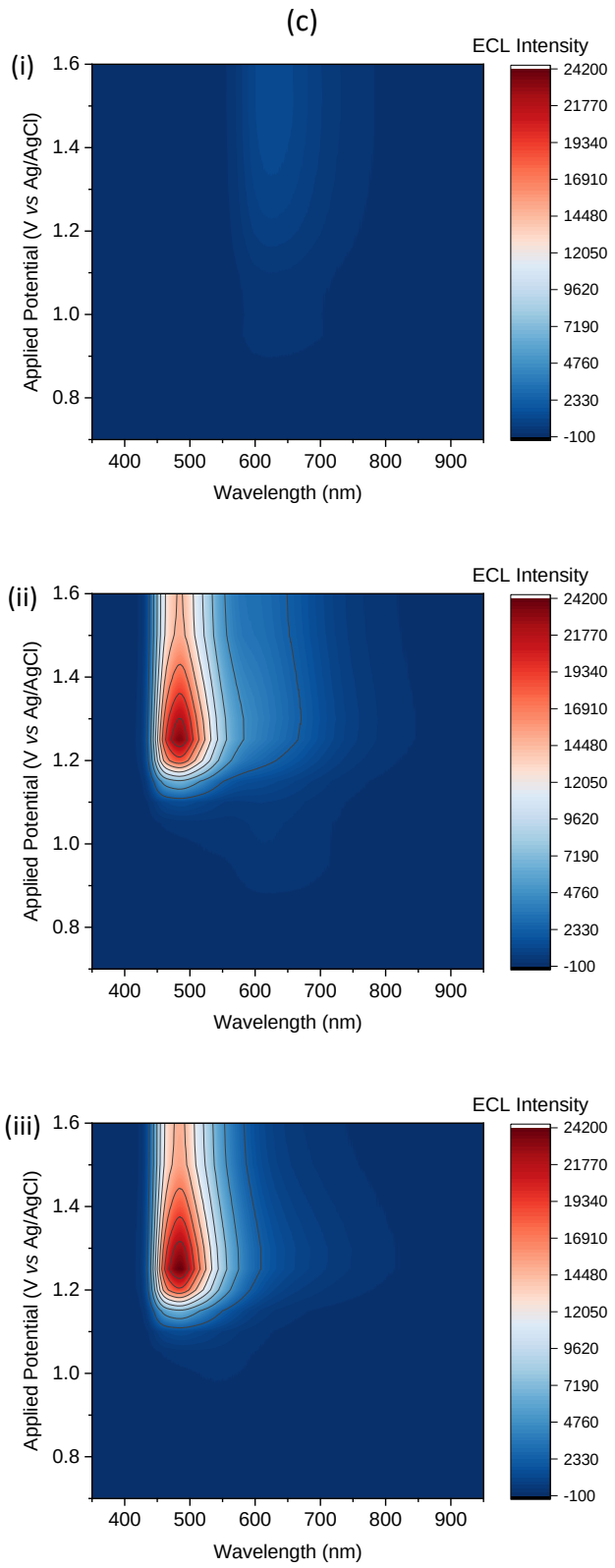
(c)
(i)
(ii)
(iii)
ECL Intensity
24200
21770
19340
16910
14480
12050
9620
7190
4760
2330
-100
Applied Potential (V vs Ag/AgCl)
1.6
1.4
1.2
1.0
0.8
400
500
600
700
800
900
Wavelength (nm)

Figure S13. ECL intensities (integrated spectral distribution) of 1 μM $[Ru(bpy)_3]^{2+}$ (solid red plots) and 100 μM (a) $[Ir(sppy)_3]^{3-}$, (b) $[Ir(f\text{-}sppy)_3]^{3-}$, or (c) $[Ir(df\text{-}sppy)_3]^{3-}$ (black plots) from a mixture of the complexes in ProCell solution, after deconvolution of their emissions at each applied potential. The dashed red plots show the corresponding ECL intensity of 1 μM $[Ru(bpy)_3]^{2+}$ in ProCell without the Ir(III) complex.

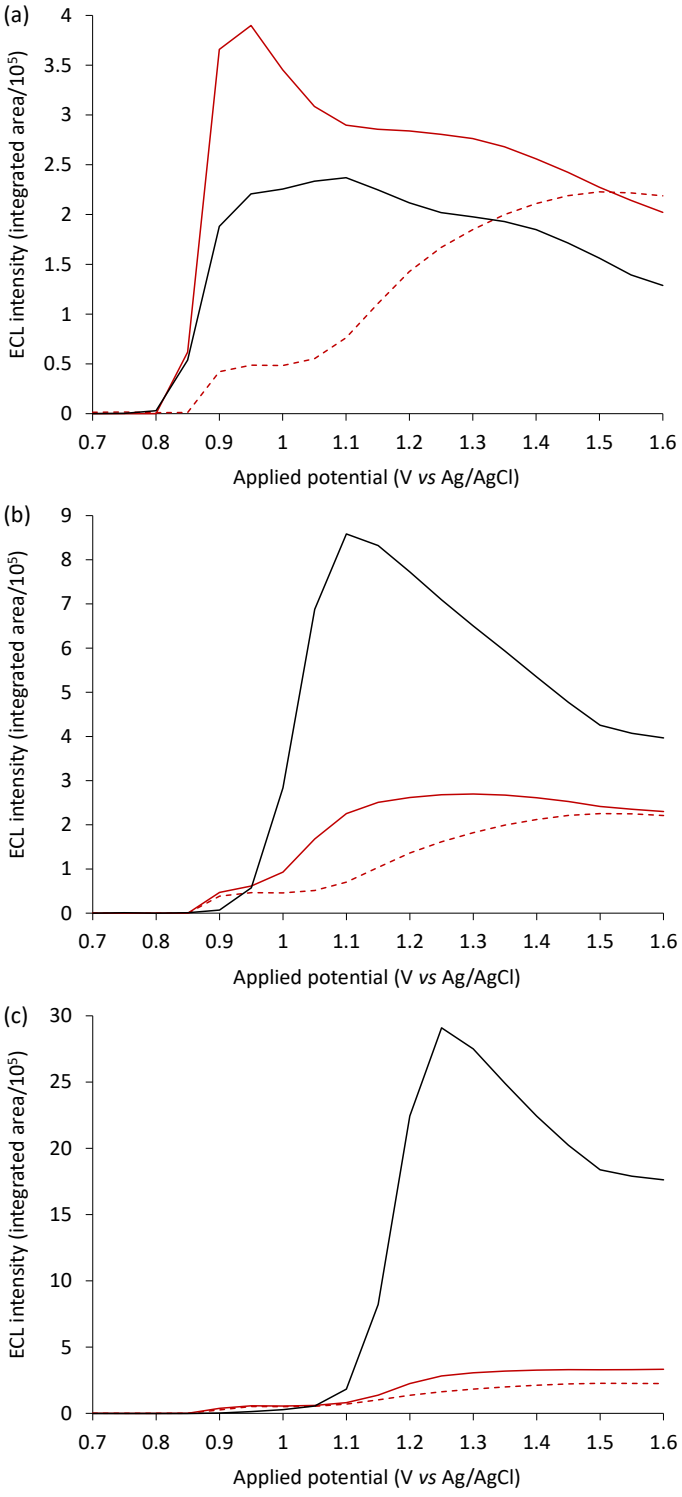

Figure S14. ECL contour plots of (i) 1 μM $[Ru(bpy)_3]^{2+}$, (ii) 1 μM $[Ru(bpy)_3]^{2+}$ and 100 μM Ir(III) complex, and (iii) 100 μM Ir(III) complex, in ProCell solution, where the Ir(III) complex is (a) $[Ir(bt)_2(pt\text{-}TEG)]^+$, (b) $[Ir(df\text{-}ppy)_2(pt\text{-}TEG)]^+$, or (c) $[Ir(ppy)_2(pt\text{-}TEG)]^+$.

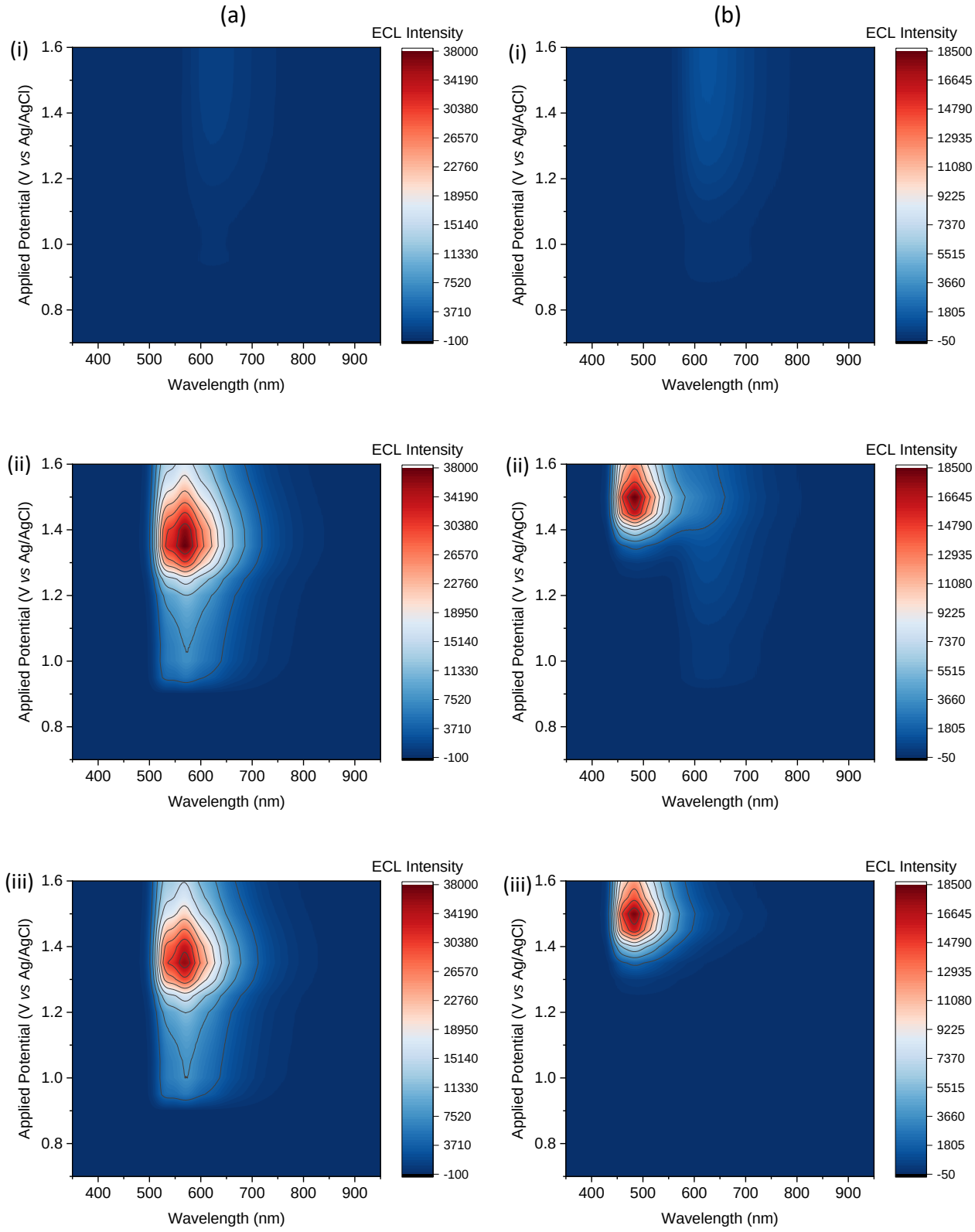

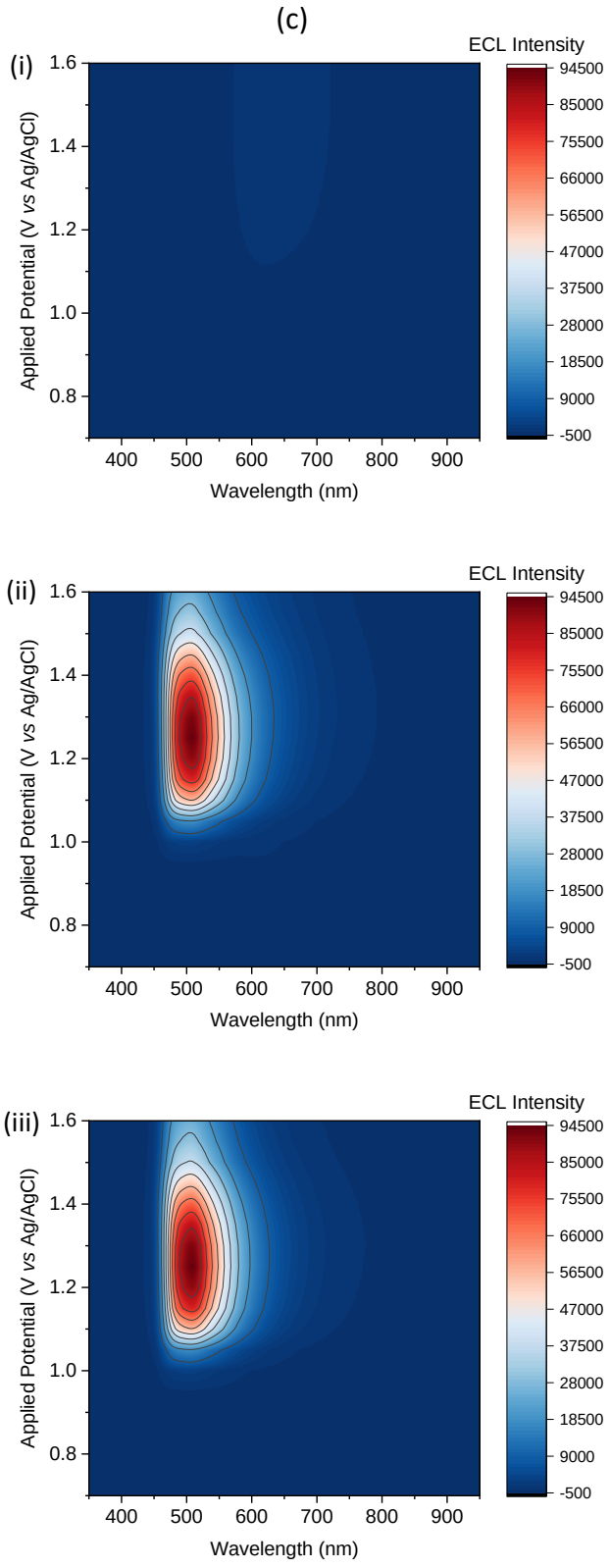
(c)
(i)
(ii)
(iii)
ECL Intensity
94500
85000
75500
66000
56500
47000
37500
28000
18500
9000
-500
Applied Potential (V vs Ag/AgCl)
1.6
1.4
1.2
1.0
0.8
400
500
600
700
800
900
Wavelength (nm)

Figure S15. ECL intensities (integrated spectral distribution) of 1 μM $[Ru(bpy)_3]^{2+}$ (solid red plots) and 100 μM (a) $[Ir(bt)_2(pt\text{-}TEG)]^+$, (b) $[Ir(df\text{-}ppy)_2(pt\text{-}TEG)]^+$, or (c) $[Ir(ppy)_2(pt\text{-}TEG)]^+$ (black plots) from a mixture of the complexes in ProCell solution, after deconvolution of their emissions at each applied potential. The dashed red plots show the corresponding ECL intensity of 1 μM $[Ru(bpy)_3]^{2+}$ in ProCell without the Ir(III) complex.

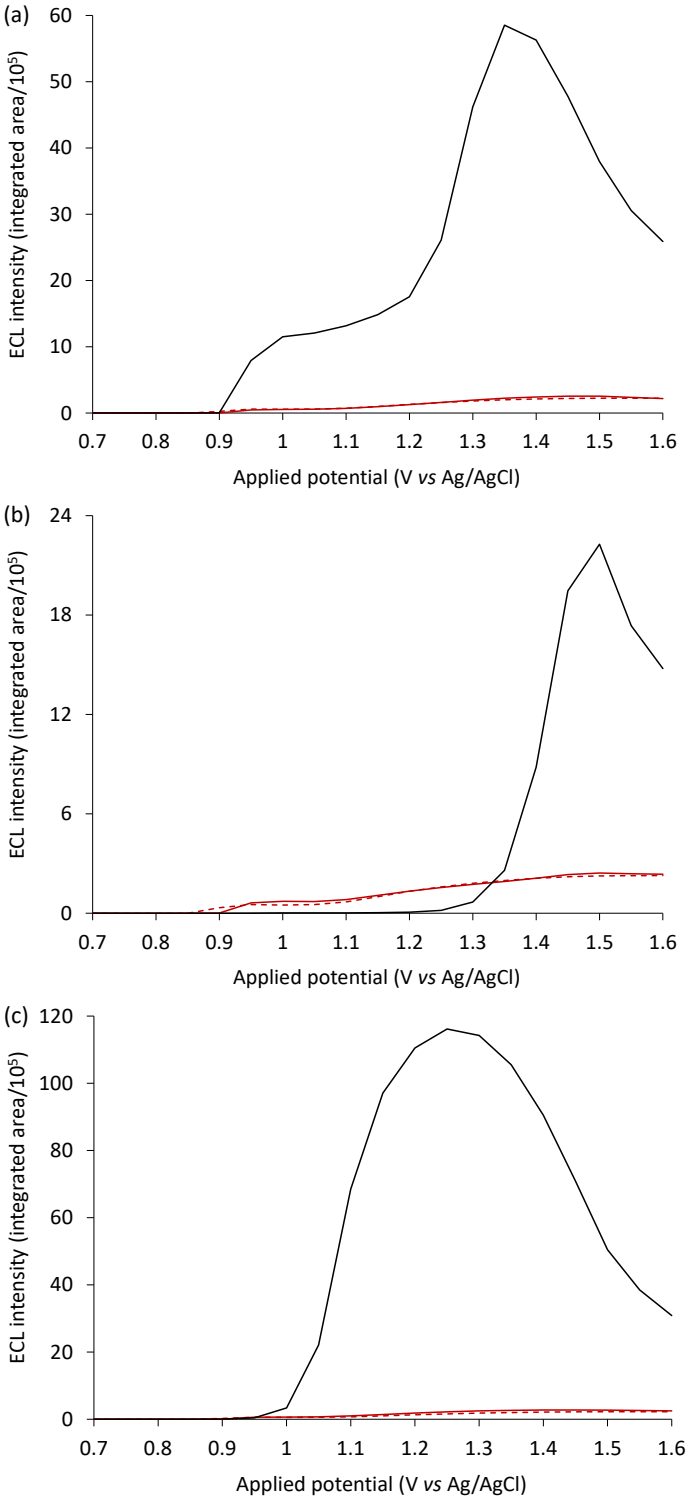

Figure S16. ECL contour plots of (i) 1 μM $[Ru(bpy)_3]^{2+}$, (ii) 1 μM $[Ru(bpy)_3]^{2+}$ and 10 μM Ir(III) complex, and (iii) 10 μM 100 μM Ir(III) complex, in ProCell solution, where the Ir(III) complex is (a) $[Ir(bt)_2(pt\text{-}TEG)]^+$, (b) $[Ir(df\text{-}ppy)_2(pt\text{-}TEG)]^+$, or (c) $[Ir(ppy)_2(pt\text{-}TEG)]^+$.

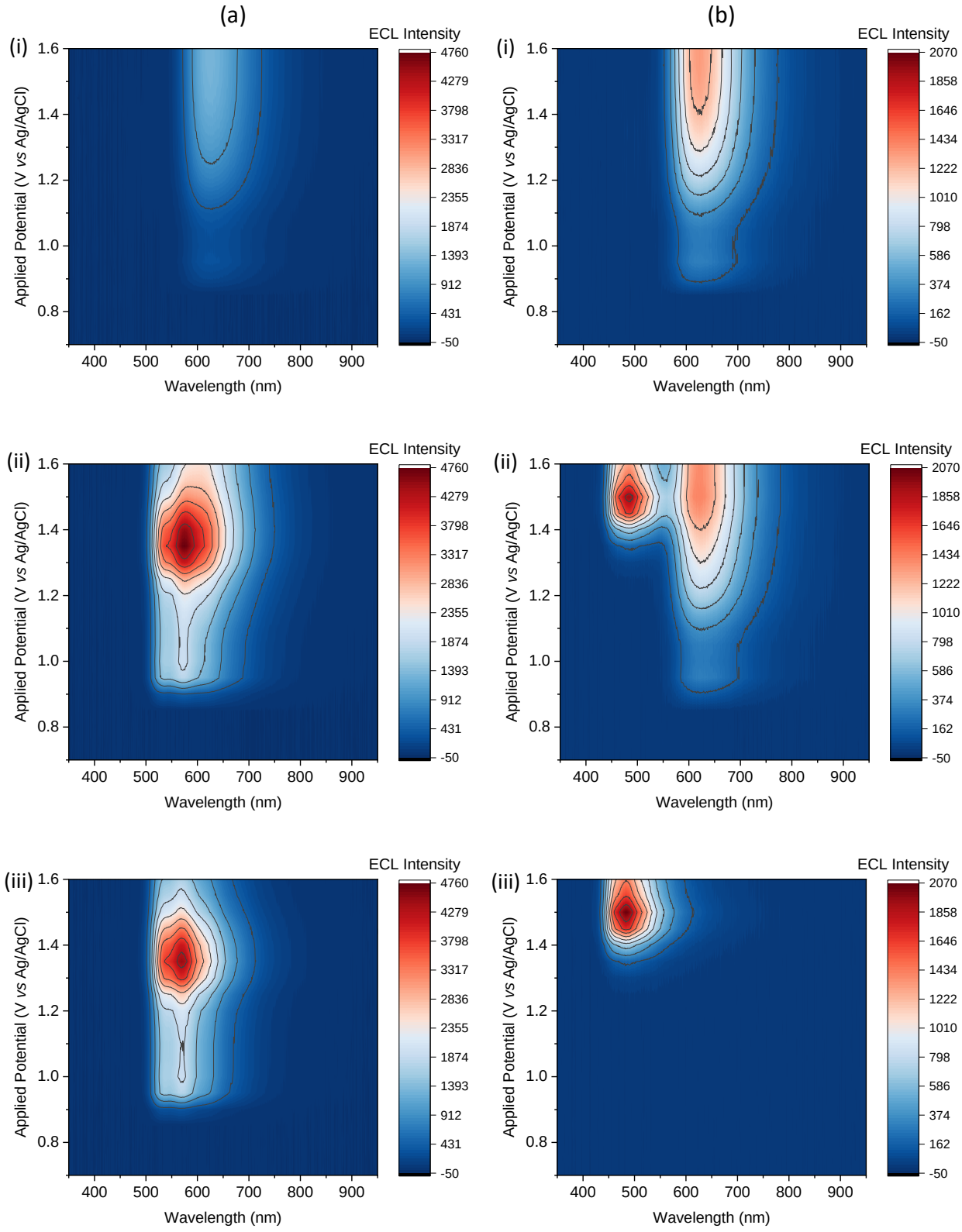

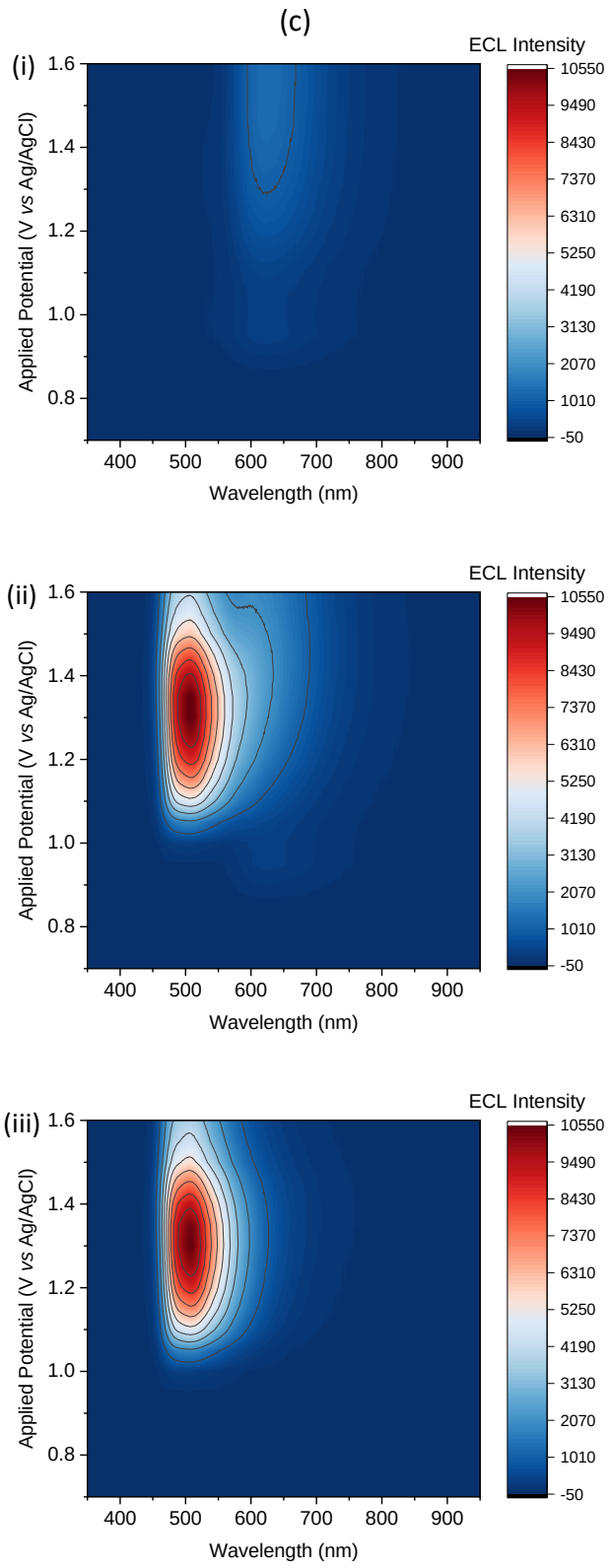
(c)
(i)
(ii)
(iii)
ECL Intensity
10550
9490
8430
7370
6310
5250
4190
3130
2070
1010
-50
Applied Potential (V vs Ag/AgCl)
1.6
1.4
1.2
1.0
0.8
400
500
600
700
800
900
Wavelength (nm)

Figure S17. ECL intensities (integrated spectral distribution) of 1 μM $[Ru(bpy)_3]^{2+}$ (solid red plots) and 10 μM (a) $[Ir(bt)_2(pt\text{-}TEG)]^+$, (b) $[Ir(df\text{-}ppy)_2(pt\text{-}TEG)]^+$, or (c) $[Ir(ppy)_2(pt\text{-}TEG)]^+$ (blue plots) from a mixture of the complexes in ProCell solution, after deconvolution of their emissions at each applied potential. The dashed red plots show the corresponding ECL intensity of 1 μM $[Ru(bpy)_3]^{2+}$ in ProCell without the Ir(III) complex.

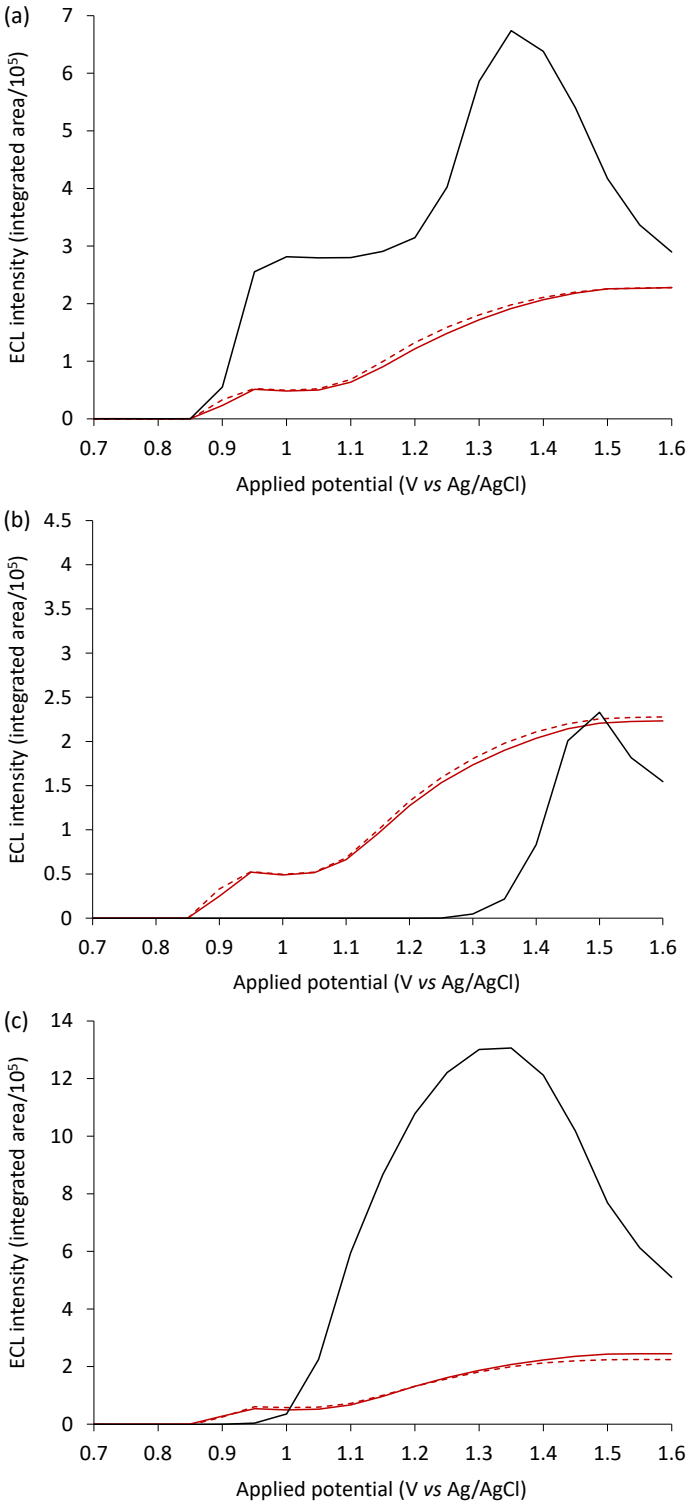

References

[1] W.E. Jones, Jr., M.A. Fox, Determination of excited-state redox potentials by phase-modulated voltammetry, J. Phys. Chem., 98 (1994) 5095-5099.

[2] L. Chen, D.J. Hayne, E.H. Doeven, J. Agugiaro, D.J.D. Wilson, L.C. Henderson, T.U. Connell, Y.H. Nai, R. Alexander, S. Carrara, C.F. Hogan, P.S. Donnelly, P.S. Francis, A conceptual framework for the development of iridium(III) complex-based electrogenerated chemiluminescence labels, Chem. Sci., 10 (2019) 8654-8667.